CO12-1 Survey on Radioactive Cesium Migration between Environment and Body of Wild Boar (*Sus scrofa*) Living in Fukushima Prefecture

M. Fukushima[1], Y. Tsuji[1], Y. Iinuma[2], H. Komatsu[3], R. Kumada[3], K. Kanda[3]

Graduate School of Science, Kyoto University

[1]Faculty of Science and Engineering, Ishinomaki Senshu University

[2]Institute for Integrated Radiation and Nuclear Science, Kyoto University

[3]Fukushima Prefectual Centre for Environmental Creation

INTRODUCTION: Migration of radioactive cesium caused by Fukushima-Daiichi Reactor accident between environment and several species of wild animals in 2011 has been studied by several groups including Fukushima Prefecture Centre for Environmental Creation. In their results, radioactive cesium levels showed correation between wild boar muscle and stomach contents[1], and it suggested that radioactive cesuim migrate from diets to wild animal bodies. Wild boar diets show seasonal changes, and it is expected that trace elements levels in wild animals show seasonal changes. For these purposes, we have analyzed several elements in muscles and gastrointestinal contents including stomach, colon, and rectum of wild boars living in Fukushima Pref.

EXPERIMENTS: Wild boars were trapped in Nihonmatsu City, Fukushima Pref. under the permission of Fukushima Pref. from May 2018 to February 2022. After euthanasia by neck shot, musclus quadriceps, contents of the stomach, colon, rectum, and the liver were removed from body, freeze-dried, pulverized, and gamma-ray counting was done for Cs-134 and Cs-137 radioactivity. Also, before freeze-drying, some amount of stomach content was kept in 70% ethanol soln. and separated each materials unter optical microscope for estimating wild boar diet. One portion of dried power was supplied for short irradiation and another portion was used for long irradiation in KUR. Eight elements of Ca, Cl, Cu, K, Mg, Mn, Na, and V were analyzed by the condition of 1.5 min TcPn irradiation, 3 min cooling time, and 10 min gannma counting using germanium detector with Compton suppression system, also eight elements of Co, Cr, Cs, Fe, Rb, Sc, Se, and Zn were irradiated for 1 hour and gamma counting was done for 20 - 30 min after 1 month cooling time. For different standard reference materials were used: NIST SRM 1575 Pine Needles, NIST SRM 1577b Bovine Liver, NIST SRM 1573a Tomato Leaves, and NIST SRM 1515 Apple Leaves.

RESULTS: **<Wild boar diet>** Stomach contents were mainly consisted by leaves, stem, and fleshy fruits for whole study periods. Roots was main diet in autumn and winter, likely due to poor fruiting of acorns, which is known as main diet of the wild boar in these seasons. **<Radioactive Cs levels between muscle and stomach content>** Correation factor (R^2) of Cs-137 levels between muscles and stomach contents for 20 wild boars showed 0.05, and it meant there is no relationship between them caught in 2021 and 2022.

<Muscle > Long irradiation was done for 25 different muscle samples and obtained 5 levels of elements. Their averages and standard deviations are shown is shown in Table 1.

Table 1. Elemental levels in wild boar muscles. (unit: mg/kg, dry weight)

	Se	Cr	Rb	Fe	Zn
Avg	0.95	0.86	21.2	92.9	109
SD	0.39	0.73	16.4	22.0	38

<Gastrointestinal contents> Long irradiation was done for 3 different gastrointestinal contents and obtained 7 elemental levels, and their averages and standard deviations are shown in Table 2.

Table 2. Elemental levels in gastrointestinal contents. (unit: mg/kg, dry weight)

Element		Se	Cr	Sc	Rb	Fe	Zn	Co
Sc[*1]	Avg	1.97	6.23	1.34	4.23	4190	30.5	1.06
	SD	2.34	6.01	0.05	7.32	260	5.9	0.16
Cc[*2]	Avg	3.78	16.5	5.53	36.9	16300	67.6	4.94
	SD	4.55	5.1	0.49	8.1	800	29.3	0.56

Sc[*1]: stomach content, Cc[*2]: colon content.

When gamma spectra were measured, high levels of photopeaks caused from Sb-124 were found, and the highest peak energy of Sb-124 is 602.7 keV, which almost overlaps with photopeak of 604 keV caused from Cs-134. Sb and high levels of Fe are supposed to be the content of soil ingested with diets such as potatos, fallen acorns, insects, and so on. For investigating the migration of radioactive Cs, equilibrium of stable Cs and radioactive Cs in both environment and diet, it is important to analyze stable Cs both in the body of wild boars and in environment. Since stable Cs changes to Cs-134 by neutron irradiation, separation of soil and diet in stomach contents is needed.

REFERENCES:

[1] Y. Nemoto *et al*., Journal of Environmental Radioactivity, **225** (2020) 106342.

CO12-2 Synthesis of high-quality crystals for laser shock experiments: Implicartions for understanding the giant planet interiors

Y. Umeda[1], Y. Seto[2], T. Sekine[3], T. Duffy[4], F. Coppari[5], R. Smith[5], and T. Okuchi[1]

[1]*Institute for Integrated Radiation and Nuclear Science, Kyoto University*
[2]*Graduate School of Science, Osaka Metropolitan University*
[3]*Center for High Pressure Science & Technology Advanced Research*
[4]*Department of Geosciences, Princeton University*
[5]*Lawrence Livermore National Laboratory*

INTRODUCTION: The properties of ferropericlase, (Mg, Fe)O, especially its phase transition from the B1 (NaCl) to the B2 (CsCl) -type structure, may play a key role in controlling the deep dynamics of many rocky exoplanets, influencing properties such as mantle viscosity, heat flow, and magnetic field generation[1,2]. However, shock wave experiments to date have focused almost exclusively on the MgO or FeO endmembers. There are very limited shock compression data on planetary-relevant intermediate (Mg, Fe)O compositions.

In this study, we synthesized the single crystal of ferropericlase with high purity and chemical uniformity to understand the interiors of giant planets with a more reasonable chemical composition. This project will provide the first experimental data for directly testing recent theoretical predictions of metallization and phase stability of this material under conditions of super-Earth interiors and provide insights into the kinetics of polymorphic phase transitions under shock compression.

EXPERIMENTS: The (100) single crystal periclase MgO plate (5 x 5 x 0.05~0.15 mm), MgO powder, and FeO powder were prepared as starting materials. At first, mixed powder in fixed FeO and MgO ratios were grounded using an agate mortar and pestle. Mixing ratio was FeO:MgO=0.11: 0.89. Pellets were made of mixed powder using pelletizer at 2 MPa. The pellets of the mixed powder were baked for 18 h at 1400ºC and CO_2=340 cc/min, H_2=80 cc/min ($logfO_2$=-7.5) in a gas-mixing furnace at Kobe university using H_2/CO_2 gases, keeping O_2 fugacity between iron-wustite (IW) and quartz-fayalite-magnetite (QFM) buffer.

In next, the MgO plates were packed by pre-synthesized $(Fe_{0.11}, Mg_{0.89})O$ powder using pelletizer. Packed pellets were backed for 30 hours at 1450ºC and CO_2=340 cc/min, H_2=80 cc/min using H_2/CO_2 gases, keeping O_2 fugacity between IW and QFM buffer. After that, we excavated the crystal and polish it for X-ray diffraction (XRD) and Scanning electron microscopy (SEM) analyses to evaluate homogeneity and chemical compositions.

RESULTS: Single crystal ferropericlase has been synthesized via the interdiffusion of Mg-Fe between MgO plates and pre-synthesized (Mg, Fe)O powder in a gas-mixing furnace (Fig. 1).

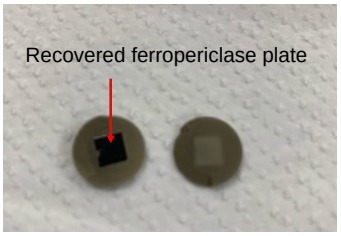

Fig. 1. Photo of single crystal ferropericlase synthesized for this study.

Scanning electron microscopy (SEM) imaging and energy dispersive X-ray (EDX) compositional analyses were performed across the short dimension of the single crystals and show that the samples are free of porosity and chemically homogenous Mg/(Mg+Fe) composition 92.9 ± 0.2 (Fig. 2).

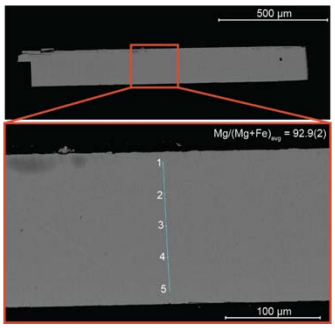

Fig. 2. SEM image of a ~100 µm thick (Mg,Fe)O single crystal synthesized in this study. Five EDX analyses were performed across the short dimension of the single crystal.

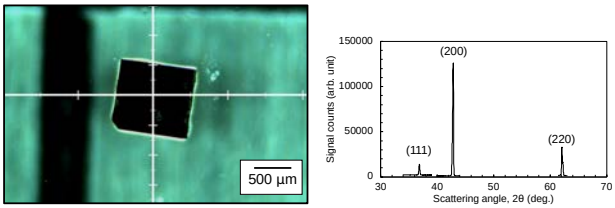

Fig. 3. Synthesized single crystal Ferropericlase, (Mg, Fe)O. X-ray diffraction profile of the synthesized crystal by micro focus XRD.

In summary, we succeeded in synthesizing the target composition $(Mg_{90}, Fe_{10})O$ of single crystal ferropericlase. The establishment of synthesis in this study is expected to enable us to obtain high-precision data for a wider range of compositions as laser shock targets.

REFERENCES:

[1] F. Coppari *et al.,* Nat. Geosci., **14** (2021) 121–126.
[2] S. Ritterbex *et al.,* Icarus, **305**, (2018) 350–357.

CO12-3 Neutron Activation Analysis of High Purity Material

T. Miura[1], S. Sekimoto[2], R. Okumura[2], H. Yoshinaga[2], Y. Iinuma[2]

[1]AIST, National Metrology Institute of Japan
[2]Institute for Integrated Radiation and Nuclear Science, Kyoto University

INTRODUCTION: National Metrology Institute of Japan (NMIJ) is responsible for developing certified reference materials and for establishing the traceability of SI (The International System of Units) on chemical metrology in Japan. To establish SI traceability, the primary method of measurements should be applied to the characterization of the certified reference materials. Neutron activation analysis using comparator standard is recognized as a potential primary ratio method [1]. Despite the potential of neutron activation analysis as primary ratio method, the evaluation the measurement capability and the measurement uncertainty are required in any analysis. In general, there are three main components of uncertainty in neutron activation analysis, that is, sample preparation uncertainty, neutron flux homogeneity, and gamma ray measurement uncertainty. Usually, flux monitor is used to correct the neutron flux heterogeneity. However, although the flux monitor can correct the neutron flux variation using the count rate of the known amount of the monitor nuclide, it does not reflect the neutron flux of the actual sample. The most practical method to eliminate neutron flux heterogeneity to improve gamma ray measurement uncertainty is an internal standard method [2, 3]. For the development of primary inorganic standard solution as national standard, the purity of starting material must be determined. The high purity yttrium oxide was candidate starting material for preparation of Y standard solution as national standard of Japan. The several trace analytical methods including neutron activation analysis, were used for purity determination of the high purity yttrium oxide. In this work, we presented that capability of instrumental neutron activation analysis for determination of Sc, La, Pr, Nd, Sm, Eu, Gd, Tb, Dy, Ho, Er, Yb, and Lu as impurity about rare earth elements in the high purity yttrium oxide.

EXPERIMENTS: The high purity yttrium oxide purchased from FUJIFILM Wako Pure Chemical Corporation. The informative purity value of the yttrium oxide and neodymium oxide were 99.99 %. NIST SRM single element standard solutions (3148a Sc, 3127a La, 3142a Pr, 3135a Nd, 3147a Sm, 3117a Eu, 3118a Gd, 3157a Tb, 3115a Dy, 3123a Ho, 3116a Er, 3160a Tm, 3166a Yb, 3130a Lu) were used for calibration standard in impurity analysis of the neodymium oxide, respectively. The standard solutions were added on filter paper to prepare the calibration standard in the analysis. The prepared calibration standards were heat sealed into polyethylene bags. Ten to 100 mg of the yttrium oxide samples were used for impurity analysis. The neutron irradiations for yttrium oxide performed by KUR Pn2 (thermal neutron flux: 5.5×10^{12} $cm^{-2}s^{-1}$) for 2 h, Pn3 (thermal neutron flux: 4.7×10^{12} $cm^{-2}s^{-1}$) for 5 min. The irradiated samples were cooled appropriately. The gamma rays form irradiated samples were measured using Canberra GC4070-7500 Ge detector with Laboratory Equipment Corporation MCA 600. The measure radioactive isotopes were ^{46}Sc, ^{140}La, ^{141}Ce, ^{142}Pr, ^{147}Nd, ^{153}Sm, ^{152}Eu, ^{159}Gd, ^{160}Tb, ^{165}Dy, ^{166}Ho, ^{171}Er, ^{170}Tm, ^{175}Yb and ^{177}Lu.

RESULTS: Analytical results of the high purity yttrium oxide were shown in Table 1. In this measurement, Sc, La, Ce, Pr, Nd, Sm, Eu, Gd, Tb, Dy, Ho, Er, Yb, and Lu in the yttrium oxide sample could not be detected by instrumental neutron activation analysis. Therefore, the detection limits for these elements were estimate from the count rate of energy region of gamma rays emitted by induced radioactive nuclides. The estimated detection limits were also presented on Table 1. The analytical results show the useful analytical capability of neutron activation analysis for the impurity analysis of the high purity yttrium oxide.

Table 1. Analytical results of the high purity yttrium oxide.

	Yttrium oxide
	Measured values, mg/kg
Sc	$< 3.6\times10^{-4}$
La	$< 1.6\times10^{-2}$
Ce	$< 8.8\times10^{-2}$
Pr	$< 7\times10^{-3}$
Nd	< 1.1
Sm	< 0.17
Eu	$< 2.3\times10^{-3}$
Gd	< 0.15
Tb	$< 1.9\times10^{-3}$
Dy	$< 3.6\times10^{-3}$
Ho	< 0.36
Er	< 0.48
Tm	$< 2.4\times10^{-2}$
Yb	< 0.5
Lu	$< 1.5\times10^{-2}$

REFERENCES:

[1] R. Greenberg, Spectrochim. Acta B, **66** (2011) 193-241.
[2] T. Miura *et al.,* Talanta, **82** (2010) 1143-1148.
[3] T. Miura *et al.,* J. Radioanal. Nucl. Chem., **303** (2015) 1417-1420.
[4] NuDat 2, National Nuclear Data Center in Brookhaven National Laboratory, https://www.nndc.bnl.gov/nudat2/index.jsp.

CO12-4 Development of Value assignment method of Uranium Solution

T. Miura[1] and K. Takamiya[2]

[1]*AIST, National Metrology Institute of Japan*
[2]*Institute for Integrated Radiation and Nuclear Science, Kyoto University*

INTRODUCTION:

National Metrology Institute of Japan (NMIJ) is responsible for developing certified reference materials and for establishing the traceability of SI (The International System of Units) on chemical metrology in Japan. To establish SI traceability, the primary method of measurements should be applied to the characterization of the certified reference materials[1)]. Gravimetric analysis[2)], titration method[1)], and coulometric analysis are recognized primary method for high purity inorganic material or inorganic standard solution. In this study, EDTA (ethylenediamine-*N*, *N*, *N*', *N*'-tetra-acetic acid) chelatometric titration method was applied for determination of U in solution sample. Uranyl ion is difficult to titrate with EDTA because of its small complexation constant with EDTA. On the other hand, the logarithm of the stability constant between U(IV) and EDTA (Log $K_{U(IV)Y}$) is about 25, which allows titration at low pH (pH 1 to 3) where there is little interference from coexisting metal ions.

REAGENTS and INSTRUMENTS:

The 100 g of U solution was prepared by dissolving the 0.2 g of Uranium oxide (Mitsuwa Chemical Co.Ltd., Osaka, Japan) using nitric acid. Dojindo Laboratories EDTA and Xylenol orange (XO) were purchased from FUJIFILM Wako Pure Chemicals Corporation. NMIJ CRM Bi standard solution was used for back titration. Other chemical reagents (nitric acid, acetic acid, ammonium acetate, ascorbic acid, etc.,) were analytical grade or JIS special grade. AT-510 automatic titrator (Kyoto Electronics Manufacturing Co., Ltd, Kyoto, Japan) was used for titration for U in the sample solution. ATX324 chemical balance (Shimadzu Corporation, Kyoto, Japan) was used to sample weighing. HM-30 pH meter (TOA-DKK, Tokyo, Japan) were used for pH measurement.

TITRATION METHOD:

The pH of the sample solution was adjusted from 3 to 4 by dropping ammonium acetate solution into the sample solution containing about 2 mg of uranyl ion. Excess amounts of EDTA standard solution (0.01 mol/kg) and ascorbic acid (100 mg) were added to the sample solution. The sample solution was then heated and boiled on a hot plate for approximately 10 minutes to form the U(IV)-EDTA complex. After the sample solution was cooled to room temperature, acetic acid was added to the sample solution to adjust the pH from 2 to 3. Finally, 0.01 % XO indicator solution was added to the sample solution and back titrated with 0.01 mol/kg Bi standard solution.

RESULTS:

Analytical results of the U in the sample solution by EDTA titration method were shown in Table 1. In this experiment, titration was performed by changing the pH of the sample solution in steps from 2 to 3. The experimental results showed that the effect of pH was small in this pH range. From this titration experiment, it was verified that the EDTA titration method can be determined a small amount of uranium (about 2 mg) with a repeatability of less than 0.2%.

Table 1. Analytical results of the U in the sample solution.

Run No.	pH	U mg/kg
1	3.00	1851
2	2.86	1850
3	2.73	1849
4	2.62	1854
5	2.55	1858
6	2.41	1852
7	2.32	1846
8	2.27	1853
9	2.22	1854
	Mean	1852
	RSD	0.185 %

REFERENCES:

[1] J. Vogl *et al*., Metrologia, **55** (2018) 211.
[2] T. Miura and A. Wada, Front. Chem., (2022) 88863.
[3] J. Kinnunen and B. Wennerstrand, Chem. Anal., **46** (1957) 92.

CO12-5 Experimental Study of Superposition of Coherent Transition Radiation Using a Ring-type Resonator

N. Sei and T. Takahashi[1]

Research Institute for Measurement and Analytical Instrumentation, National Institute of Advanced Industrial Science and Technology

[1]Institute for Integrated Radiation and Nuclear Science, Kyoto University

INTRODUCTION: Nonlinear optical phenomena such as hole burning [1], which were once popular in the infrared region, have been studied in the terahertz region, and terahertz light sources with high peak power are desired. To meet this requirement using high-energy electron beams, we have developed a technique of pulse superposition of coherent transition radiation (CTR) using a ring-type resonator. By orbiting the ring-type resonator, the electric field of the CTR micropulses is superimposed, and the peak power of the CTR increases nonlinearly. We installed a ring-type resonator in the electron beam orbit and inserted a cyclo-olefin polymer substrate into the resonator as an output coupler. By inserting a millimeter-wave absorber into the resonator, we confirmed that the CTR accumulated in the resonator. The power of the CTR micropulse increased approximately twice in spite of a large cavity loss, and the experimental results suggest that the electric field of the CTR micropulses were superimposed in positive phase.

EXPERIMENTS: An electron beam with the energy of 39 MeV and the average current of 1.8 μA was used for the experiments at L-band linac of Kyoto University. The reputation frequency of the electron-beam macropulse was 15 Hz. Because the macropulse duration was 100 ns, the number of electron-beam micropulse in a macropulse was 130. Schematic layout of the ring-type resonator used in the experiments is shown in Fig. 1. The electron beam generated CTR at two thin polyethylene films vapor-deposited with aluminum when it passed through them. The thickness of the polyethylene film was 6 μm. These polyethylene films were also used as mirrors constituting the resonator. The two CTR beams were confined in the resonator composed of four mirrors, which included two parabolic mirrors with the focal length of 508 mm. The cavity length of the resonator was 922 mm, which was four times the interval of the electron bunches. The downstream parabolic mirror was mounted on a linear stage and the cavity length could be adjusted. In order to extract the resonate CTR beam from the resonator, a cyclo-olefin polymer substrate with a thickness of 3 mm was inserted into the resonator at an angle of 45 degrees with respect to the optical axis. The cyclo-olefin polymer was almost transparent in a frequency range below 1 THz, and its refractive index was 1.53 [2]. The extraction efficiency for the CTR beam due to reflection on the front and back of the substrate was approximately 10%.

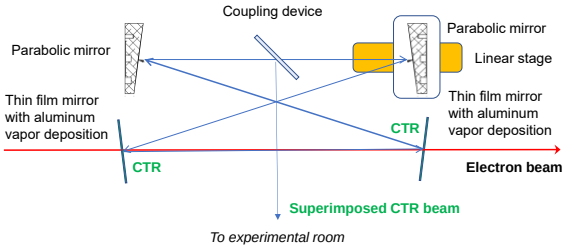

Fig. 1. Schematic layout of the ring-type resonator.

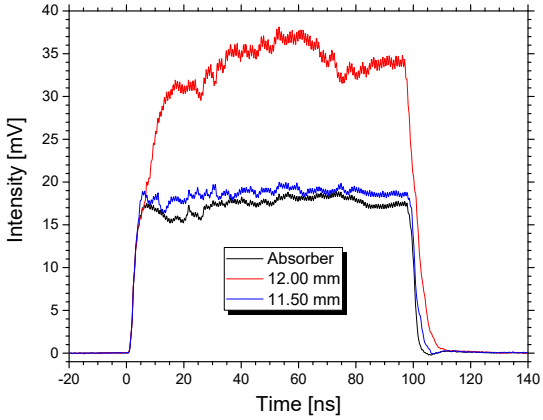

Fig. 2. Measured temporal evolution of the horizontal component of CTR micropulse power.

RESULTS: The CTR beam transported to the experimental room was measured by a D-band diode detector (Millitech Inc., DXP-06). Figure 2 shows temporal evolution of the horizontal component of the CTR micropulse. When a scale of the linear stage was 12.00 mm, the power of the resonated CTR micropulse was approximately twice that inserting a millimeter-wave absorber in the resonator. When the stage was moved by -0.5 mm, the CTR power decreased to almost the same power with the absorber. This variation of the power of the CTR micropulse suggests that the longitudinal mode appeared due to the change of the cavity length. Therefore, it was confirmed that the electric field of the CTR micropulses was superimposed by the resonator positively.

In these experiments, the amplification of the CTR micropulse power caused by the pulse superposition was insufficient due to the large cavity loss of the resonator. We are planning to remodel the resonator so that the superposition rate can be increased.

REFERENCES:

[1] J. Dong *et al.*, Opt. Rev., **15**, (2008) 57–74.
[2] E. Mavrona, Opt. Mat. Express, **11** (2021) 2495-2504.

CO12-6 The Third-year Trial to Analyze the Texture of Roof-tile: Toward Detailed Provenancial Studies of Excavated Ceramics by INAA

M. Tomii, K. Takamiya[1], H. Yoshii[2], M. Kidachi[3], Y. Chiba[2], and A. Ito[2]

Faculty of Literature, Taisho University
[1]Institute for Integrated Radiation and Nuclear Science, Kyoto University
[2] Graduate School of Letters, Kyoto University
[3] College of Letters, Ritsumeikan University

INTRODUCTION: Aiming to establish the procedures to archaeologically identify local groups for production of ceramics in Japan, 20 pieces of the roof-tiles with stamp impression from the same collection as the one in the first year are analyzed this year. They were excavated from the archaeological site in the Kyoto University campus in 1992, where the garrison from the *Tosa* domain had temporally occupied in 1860s. The roof-tiles in the collection is almost exclusively composed of the ones having the stamp impressions, each of which indicates the name of maker/atelier of the tile. There are 24 kinds of stamp impression of Chinese characters, and 23 stamp impression groups of them suggest the makers in *Tosa* region respectively [1], though there is no difference in size, production technique, and the appearance of texture. This study tries to check whether the stamp impression groups correspond with the groups of tile texture in detail, to consider whether all these roof-tiles were produced at local ateliers.

EXPERIMENTS: Conventional INAA was applied to determine the elemental composition of samples of the tiles, each of which had been drilled into a fine powder as a sample and then had been enclosed in a polyethylene bag [2]. 18 pieces of the roof-tile of normal (right-sloping) type, composed of two stamp impression groups, were chosen; ten were from the "AKANOGIN" group and the others from "KATATSUNE" group. Five tiles of each group are of normal type. Another five of AKANOGIN are of left-sloping type. Among the rest three of KATATSUNE, one is of left-sloping type, and the other two are of façade-placed tiles; the decoration of the façade side of such tiles had been made with mould, meaning that this part might require finer clay through elutriation. One of the two façade tiles for analysis is of right-sloping, and another is of left-sloping, both of which serve two samples, respectively, from façade side and from back side.

Each 20 samples was neutron-irradiated, firstly at Pn-3 (1 MW for 90 seconds) to detect short-lived nuclides, and then at Pn-2 (1MW for 2 hours) to determine long-lived nuclides. The comparative standards (JR-3, JB-1b) were irradiated with the same condition. 15 mg was used for Pn-3 and 45 mg for Pn-2, in each sample.

The gamma-ray spectrometry of the irradiated samples for long-lived nuclides was performed one time (after around 30 days), while that for short-lived nuclides was done four times: just after the irradiation, after 15 minutes, 40 minutes, and around 24 hours. The photo-peak analysis was performed by using FitzPeaks [3]. Concentrations of elements included in the samples were estimated by comparison of the intensity of gamma-rays between the comparative standard and tile samples.

RESULTS: Concentrations of ten elements (Al, V, Ti, Mg, Mn, K, Ga, Na, Sm and La) in every sample were determined with irradiation by Pn-3. With irradiation by Pn-2, concentrations of twelve elements (Yb, Lu, Nd, Rb, Ce, Hf, Fe, Tb, Sc, Ta, Cs and Eu) would be determined in every sample, though the determination has not been fully completed in all samples so far. Nevertheless, the following two results can be pointed out;

a) two elements (Na and Mn) show clear difference in concentration to divide 20 samples into two groups, respectively, and the two groups fully correspond with the stamp groups (Fig.1).

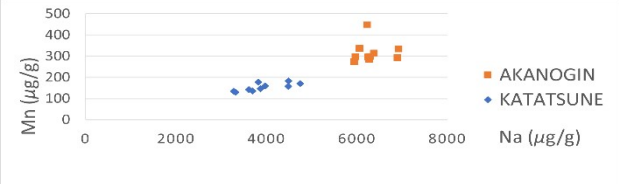

Fig. 1. Distribution of 20 samples on the concentrations combination of Na with Mn.

b) Fe does not show clear difference in concentration among the KATATSUNE groups. This might tell that elutriation for finer clay had not been operated. This atelier might use the same texture for all types (Fig.2).

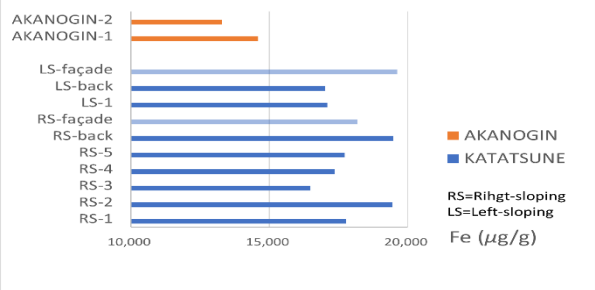

Fig. 2. Mean values of Fe of the KATATSUNE group (with the examples of the AKANOGIN group for comparison).

ACKNOWLEDGEMENT
We would like to thank Dr Johannes Sterba and Dr Maria Shinoto for advising the sampling procedures on the sherds according to the workflow established in Vienna.

REFERENCES:

[1] Y. Chiba et al., Annual Report of Archaeological Researches in KU sites for 1992., (1995) 65-125.
[2] J. Sterba, J. Radio. Nucl. Chem., 316 (2018) 753-759.
[3] J. Fitzgerald, Fitz Peaks Gamma Analysis and Calibration Software, https://www.jimfitz.co.uk/fitzpeak.htm.

CO12-7 Study for activity measurement techique of radioactive xenon gases using a plastic scintillator

T. Yamada[1,2], K. Mori[2], R. Furukawa[3] , H. Yashima[4]

Kindai University
[1]Atomic Energy Research Institute
[2]Graduate school of Science and Engineering
[3]National Metrology Institute of Japan
[4]Institute for Integrated Radiation and Nuclear Science, Kyoto University

INTRODUCTION: In order to calibrate monitors used for measuring radioactive xenon isotopes in nuclear facilities, use of activity reference measurement standard gases shall be required. A β-ray counting technique using a set of multiple ventilated proportional counters having different lengths is generally used to determine activity concentration of standard gases [1]. In this study, a method based on the 4πβ-γ spectroscopy method using a plastic scintillator (PS) as a β-detector was carried out to determine β-counting efficiency of ^{133}Xe absolutely as an alternative approach.

EXPERIMENTS: ^{133}Xe gas was produced via ^{132}Xe(n,γ)^{133}Xe reaction. Naturally occurring xenon gas consists of seven stable isotopes was filled into the small acryl container having 10 ml with atmospheric pressure and was irradiated for 60 s at the bottom of KUR-SLY under operating at 1 MW thermal output. Around 3 kBq of ^{133}Xe was produced with 7.84×10^{11} $n^{-1}s^{-1}cm^{-2}$ of the nominal flux of the thermal neutron.

A small acrylic gas container with internal dimensions of φ60 mm × 40 mm (113 ml) was used as the β-detection part of the measurement system. The entire inner wall of the container was lined with 1 mm thick of PS. The container was covered with aluminum tape on the sides and white tape on the top as a reflector, and a photomultiplier tube (PMT) was connected to the top of the container and stored in a light-shielded case. The β-detector was placed directly onto the Ge detector, and the signal outputs from the β- and γ-detectors were fed to the signal inputs of a list-mode multi-channel analyzer (MCA) capable of acquiring data in list mode to obtain list data consisting of the pulse height from each detector and a time stamp of the detection time.^{133}Xe emits γ-ray (E_γ=81 keV) following disintegration by beta minus decay to excited levels of ^{133}Cs with branching ratio of 0.9912 [2]. In order to obtain the β-γ coincidence spectrum from the time-stamped pulse height data, the γ- signals derived within 4.5 μs from the β-detection time stamps were considered as true coincidences. β-counting efficiency ε_β is determined as the ratio of net peak area in the coincidence spectrum n_c to the net peak area n_γ in the γ-spectrum. The use of naturally occurring xenon gas consists of seven stable isotopes could produce impurities of ^{129m}Xe, ^{131m}Xe, ^{133m}Xe, ^{135m}Xe, ^{135}Xe and ^{137}Xe. In the present study measurements were carried out 2 days after the end of irradiation, although there exist impurities (≈ 30 % or less) of ^{129m}Xe, ^{131m}Xe, ^{133m}Xe and ^{135}Xe.

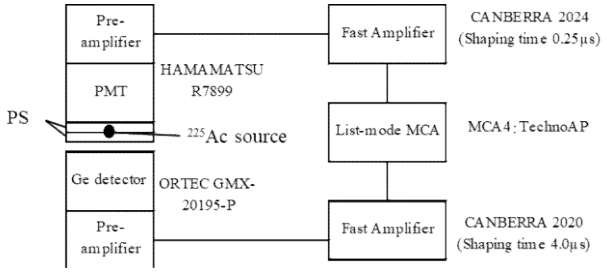

Fig. 1. Schematic diagram of the 4πβ-γ coincidence spectroscopy system used in the present study.

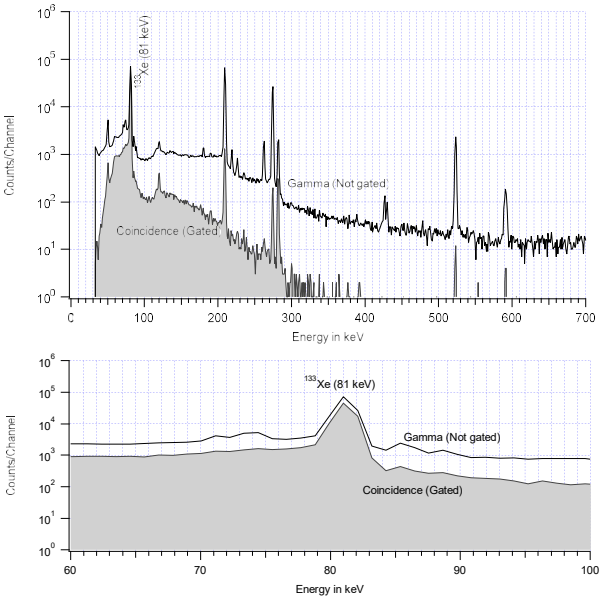

Fig. 1. Coincidence- and γ-spectra obtained from the present measurement.

RESULTS: Figure 1 shows the coincidence and γ-ray spectra obtained in the present experiment. β-counting efficiency determined as n_c / n_γ was 0.667±0.004. Even though around 0.9 of detection efficiency was obtainable for ^{41}Ar by use of the same β-counter in the previous study [3], significant loss of detection efficiency was found for ^{133}Xe. Further study should be needed to determine the cause of decrease in counting efficiency and to improve it.

REFERENCES:

[1] A. Yunoki *et al.*, KURNS Progress Report 2020 (2021) CO12-12 (R2116).
[2] Bé, M., 2011. Table of Radionuclides. http://www.nucleide.org/DDEP_WG/DDEPdata.htm.
[3] T. Yamada *et al.*, KURNS Progress Report 2021, (2022), CO12-9 (R3100).

CO12-8 Development of Compensation Method for Faster Measurement with SPND

C. H. Pyeon[1], R. Okumura[1], M. Sasano[2], R. Tanaka[3], T. Azuma[2] and M. Hayashi[2]

[1] *Institute for Integrated Radiation and Nuclear Science, Kyoto University*
[2] *Advanced Technology R&D Center, Mitsubishi Electric Corporation*
[3] *Energy Systems Center, Mitsubishi Electric Corporation*

INTRODUCTION: For safety monitoring and control of conventional pressurized water reactors, neuron signals are mainly measured from outside the reactor. For safer reactor control, constant neutron monitoring inside the reactor is required in the future. The self-powered neutron detector (SPND) is the detector that attains signals from β-decay associated with activation as a current, and outputs a current within 10 nA at 10^{12} nv. SPND is suitable for measurement in high-intensity neutron environments, but the delay in detector response due to the half-life of β-decay is one of the main technical issues in this study. We evaluated then techniques to compensate for the delay in the SPDN detector response.

EXPERIMENTS: Measurements were conducted on two days, 2023/01/12 and 2023/01/19. At the first one, we evaluated the detector power during the 0.1 MW operation. In addition, experimental data were acquired on the detector response during the start-up of the reactor and the increase in power up to 5 MW. On the second day, the detector output at 1 MW reactor power was acquired. From these data, we evaluated the compensated detector response and the linearity of the detector against the reactor power.

RESULTS: The results of plotting the SPND output, when the reactor was ramped up to 5 MW of power from the startup of the reactor, show that the detector output was raised with a delay of only 40 s and 4.4 min half-life of ^{104}Rh and ^{104m}Rh, respectively, and the time response of the SPND is 4.4 min. The gap between raw output and reactor power was over 100 s. To correct for this time response, calculations were based on the following ^{104}Rh and ^{104m}Rh β-decay. The correction can be made by deriving f in Eqs. (1) and (2).

$$N_{Rh^{104}} = -\lambda_{Rh^{104}} N_{Rh^{104}} + \lambda_{Rh^{104m}} N_{Rh^{104m}} + N_{Rh^{103}} \sigma f \quad , \quad (1)$$

$$N_{Rh^{104}} = -\lambda_{Rh^{104m}} N_{Rh^{104m}} + N_{Rh^{103}} \sigma f \quad . \quad (2)$$

Figure 1. shows the time variation of the raw detector output and the compensated one. The maximum rate of increase in reactor output is 0.045 MW/s. There was a slight delay in the maximum increase in reactor power. However, after reaching the maximum output, it was confirmed that the correction came with a delay of about 10 s or less. Also, when the increase rate of reactor output is 0.02 MW/s or less, the compensated output was observed to be followed within 5%. This is a significant improvement over the delay less than 100 s in the uncompensated data. In Fig. 2., the SPND current data obtained in the three reactor outputs were found, 0.1, 1.0 and 5.0 MW. The plots of current output versus 0.1, 1.0, and 5.0 MW are shown in Fig. 3. The results revealed that the outputs have a linearity tendency between 0.1 and 5.0 MW.

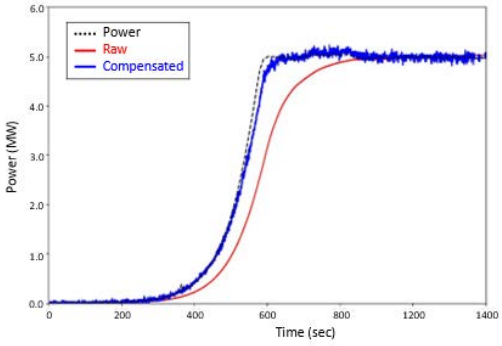

Fig. 1. The plot of normalized SPND measured current (red and blue lines mean raw and compensated, respectively) and the reactor power via time.

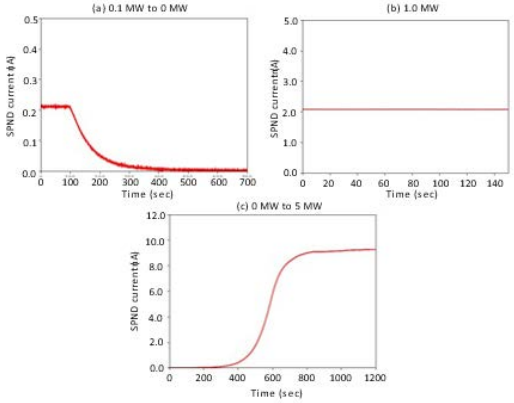

Fig. 2. The plot of SPND measured current with three conditions. (a): 0.1 MW to 0.0 MW, (b): 1.0 MW and (c): 0.0 to 5.0 MW

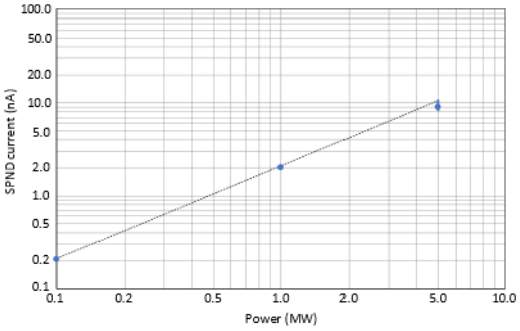

Fig. 3. The linearity of SPND output current. The plot of the current via KUR reactor power.

CO12-9 SEM-EDS analysis of sprayed and dried particles from fine particles of $(U,Zr)O_2$ for decommissioning of Fukushima Daiichi Nuclear Power Plant

A. Toyoshima, K. Takamiya[1], K. Nagata[2], and H. Furutani[3]

Institute for Radiation Sciences, Osaka University
[1]Institute for Integrated Radiation and Nuclear Science, Kyoto University
[2]Graduate School of Science, Osaka University
[3]Center for Scientific Instrument Renovation and Manufacturing Support, Osaka University

INTRODUCTION: First preliminary removal of the fuel debris remaining in the reactors of Fukushima Daiichi Nuclear Power Plant is planned to be started soon. In the removal, however, fine particles containing such as ^{235}U and ^{239}Pu are concerned to be yielded in the cutting process of the debris. We are therefore developing a novel real-time detection method of the dispersed fine particles using Aerosol Time-Of-Flight Mass Spectrometer (ATOFMS). At present, we are developing an enlargement and condensation apparatus to increase the detection sensitivity of ATOFMS by enlarging its non-detectable tiny particles to detectable-sized ones before the ATOFMS measurement. Previously, we performed SEM-EDS measurement of modeled fine particles containing ^{238}U without its enlargement. In the present study, we carried out SEM-EDS for enlarged ^{238}U particles using the developing apparatus.

EXPERIMENTS: Fine particles were prepared separately from $(U,Zr)O_2$ pellets as well as a ZrO_2 one by laser ablation. Laser power was approximately 30 mW. In a closed chamber, the pellet was irradiated by the laser. The yielded fine particles were swept out of the chamber by carrier gas of dried air and were continuously collected in water using PILS (Particle Into Liquid Sampler, Metrohm AG). The solution containing fine particles were sprayed using the developing enlargement and condensation apparatus. Polystyrene latex (PLS) standard particles were also sprayed as references. Sprayed droplets were then dried by dried air (carrier gas) and diffusion dryers. The resulting dried particles were then collected on a carbon tape set in a small impactor. SEM-EDS measurement of the collected samples was carried out after the transportation of those to KURNS. Energy of bombarded electrons was 10 kV or 15 kV. SEM images and X-ray spectra of the samples were taken for a thousand of fine particles found on the carbon tapes.

RESULTS: In Fig. 1, a SEM image of the standard fine particles with a diameter of 150 nm is shown. Many of PSL standard particles are observed. Some of these particles form aggregated clusters which are enlarged with the developed apparatus. As shown in Fig. 2, we also found similar aggregated clusters made from the U/Zr particles, element composition of which was obtained by the EDS analysis, although the amount of the enlarged particles is small. This is our first successful result on preparation of enlarged particles consisting of the tiny U/Zr particles. In the future, we will improve the enlargement and condensation apparatus for the increase of condensation efficiency.

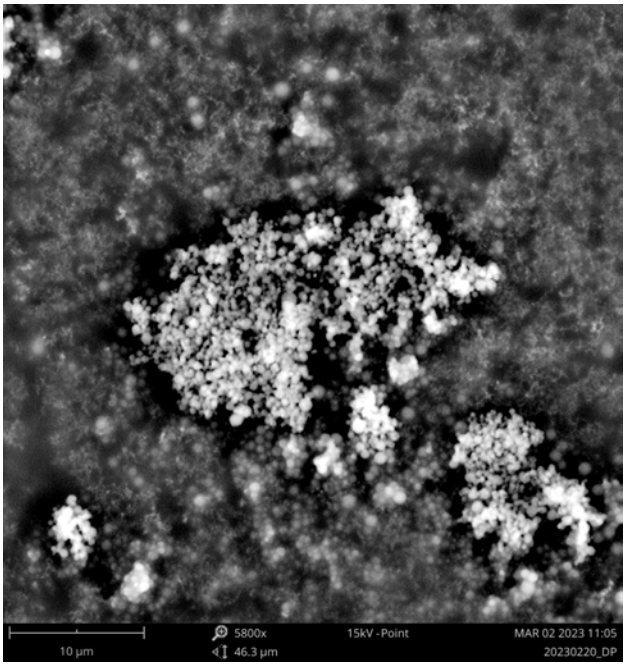

Fig. 1. SEM image of PSL particles.

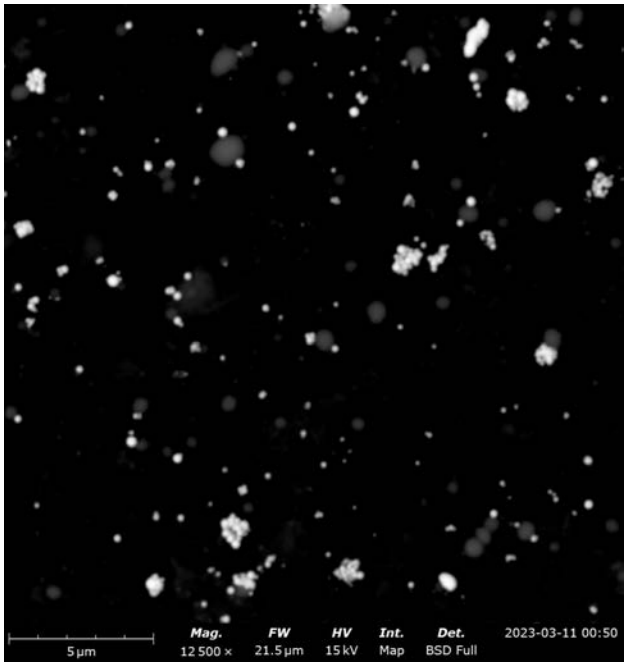

Fig. 2. SEM image of U/Zr particles.

CO12-10 Testing of a N_2-NBM readout setup at KUR CN-3

H. Ohshita, H. Endo, T. Seya, S. Matoba, M. Hino[1]

Institute of Materials Structure Science, KEK
[1]Institute of Integrated Radiation and Nuclear Science, Kyoto University

INTRODUCTION: With the advent of high-intensity pulsed neutron-source facilities, such as the Materials and Life Science Experimental Facility (MLF) at J-PARC, neutron detectors with high counting rate characteristics are required. Neutron beam monitors filled with nitrogen gas (N_2-NBMs) are known to operate in high-intensity neutron environments [1]. Neutrons were detected by measuring the rapidly charged particles emitted during the $^{14}N(n, p)^{14}C$ reaction. The *Q* value of the neutron reaction was 0.62 MeV, and the initial energies of the proton and ^{14}C were 0.58 MeV and 0.04 MeV, respectively. The cross section of the $^{14}N(n, p)^{14}C$ reaction for a thermal neutron of 1.8 Å is 1.91 b, which is $1/36000^{th}$ of the commonly used $^3He(n, p)^3H$ reaction cross section. Therefore, the application of neutron detectors based on the $^{14}N(n, p)^{14}C$ reaction is limited to neutron-beam monitoring in high-intensity neutron environments. However, in high-intensity pulsed neutron-source facilities such as the MLF, neutron-beam monitors with a thermal neutron efficiency lower than 10^{-5} are needed to suppress the counting rate, and N_2-NBM is the only realistic neutron detector. The N_2-NBM (E68953) produced by CANON Electron Tubes and Devices [2] was introduced at the MLF, and its active area of 65 mm × 65 mm was filled with a mixture of argon and nitrogen as the chamber gas. The filling pressures of argon and nitrogen were 786 Torr and 50 Torr, respectively. The expected thermal neutron efficiency was 3.9×10^{-6}. Figure 1 shows a typical readout setup of the N_2-NBM at the MLF, where the analog signal output from the N_2-NBM is pulse-shaped using a pre-amplifier 595H and a post-amplifier 4467A. A sufficiently long collection time was ensured in the first-stage preamplifier to collect the charges generated in the active area. The pulse-shaping time in the post-amplifier was 500 ns, which was designed for operation under a high-intensity pulsed neutron source. Finally, the analog signal was input to GateNET [3], where the time-of-flight (TOF) and pulse-height values were measured for the timing signal. GateNET is widely used at the MLF and can be easily integrated into existing neutron detector systems. This paper describes the testing of the N_2-NBM readout setup at KUR CN-3.

EXPERIMENTS: The A neutron detector was established downstream of the CN-3 beamline to measure the TOF during the testing of the N_2-NBM readout setup. The typical neutron intensity at the detector position was 694.5 neutrons/s·cm^2·MW. If an N_2-NBM is installed, an extremely long measurement time is required to obtain measurements with sufficient statistics. Therefore, in the test, a 3-helium proportional counter was used instead of an N_2-NBM (replacing the neutron detector in the setup shown in Figure 1). The other experimental conditions were the same as those used in previous neutron irradiation tests [4]. Figure 2 shows a comparison of the pulse height distributions for varying post-amplifier gains and shaping times. The distribution (black line) obtained using the settings shown in Figure 1 (gain 50; shaping time 500 ns) was used as the reference. In this distribution, the total absorption peak due to the $^3He(n, p)^3H$ reaction and the edges due to protons and tritons were visible, and good nγ discrimination was achieved. In general, a change in gain enlarges or shrinks the pulse height distribution, whereas a change in shaping time significantly distorts the distribution. The results shown in Figure 2, obtained at the same operating voltage, indicate that a good pulse height distribution can be obtained at a lower operating voltage by optimizing the readout setup parameters. By selecting a long shaping time, the operating voltage can be reduced by several hundred volts, which is expected to contribute to a longer detector life.

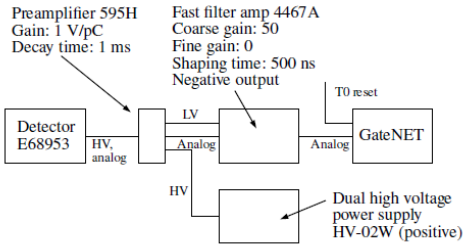

Figure 1. Typical readout setup of N_2-NBM at MLF.

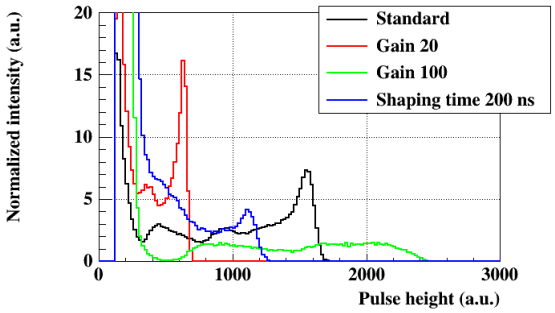

Figure 2. Comparison of pulse height distributions when the parameter settings such as gain and shaping time are varied.

REFERENCES:

[1] F. Issa, *et al.*, Phys. Rev. Accel. Beams **20** (2017) 092801.
[2] web page of CANON Electron Tubes & Devices Co., Ltd., https://etd.canon/en/index.html.
[3] S. Satoh, *et al.*, in proceedings of the ICANS XIX (2010) IP132.
[4] H. Ohshita, *et al.*, KURNS Proc. Rep. 2020 (2021) CO12-5.

CO12-11 Structural Analysis of Additives in Lubricants by Small-Angle X-ray Scattering

T. Hirayama, S. Nambo[1], W. Yagi[1], Y. Takashima[2], N. Sato[3] and M. Sugiyama[3]

Graduate School of Engineering, Kyoto University
[1]Graduate School of Engineering, Kyoto University
[2]Idemitsu Kosan Co., Ltd.
[3]Institute for Integrated Radiation and Nuclear Science, Kyoto University

INTRODUCTION: The use of low-viscosity lubricating oil is effective in reducing friction loss on sliding surfaces. However, when low-viscosity lubricating oil is used, the sliding surfaces tend to transition to a boundary lubrication state at high temperatures. Therefore, in the case of lubricating oils used over a wide temperature range, such as engine oil, it is desirable for the viscosity of the lubricating oil to change little as the temperature changes, and a polymer called a 'viscosity index improver' (VII) is added.

The structure of VII molecules in the base oil affects the viscosity characteristics of the lubricant, but it is difficult to analyze the structure of VII molecules one by one during lubricant development. Furthermore, few studies have actually analyzed the structure of VII molecules in base oils, and the relationship between the solubility of VII in base oils and its structure in base oils is unclear. In this study, we investigated the relationship between the structure of VII molecules in base oils and its solubility in base oils by dissolving VII in several base oils, analyzing the structure of VII in base oils, and evaluating the solubility of VII in base oils by the 'Hansen solubility parameter (HSP)'.

EXPERIMENT: In this study, we investigated the relationship between structure and solubility in base oils for a VII molecule called 'Comb PMA'. Five solvents were selected: tri-n-decylamine, tridodecylamine, squalane, toluene, and tetrahydrofuran. Comb PMA was dissolved in each solvent to a mass percent concentration of 2%, and SAXS measurements of Comb PMA in each solvent at 25°C were performed using a Cu small-angle X-ray scattering apparatus (NANOPIX, RIGAKU) at the Institute for Integrated Radiation and Nuclear Science, Kyoto University. The solubility of Comb PMA in solvents was evaluated using HSP, which are the solubility parameters (SP) divided into three parts: London dispersion force term, dipole inter-dipole force term, and hydrogen bonding force term, allowing for polarity that cannot be taken into account by SP values.

RESULTS: The scattering profiles obtained by SAXS measurements are shown in Fig. 1. The scattering profiles of Comb PMA in tri-n-decylamine, tridodecylamine, and squalane showed the same trend, which was different from that in toluene and tetrahydrofuran. PMA was contracted in tri-n-decylamine, tridodecylamine, and squalane, while Comb PMA was expanded in toluene and tetrahydrofuran.

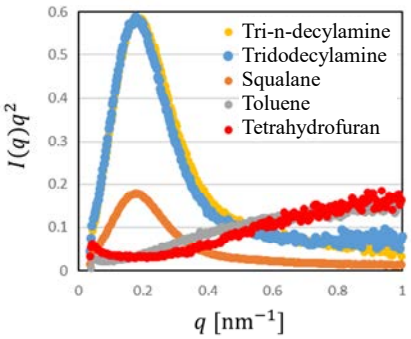

Fig.1. Kratky plots of Comb PMA in various oils.

DISCUSSION: The HSP distance between Comb PMA and each solvent was calculated, and the order of HSP distance from shortest to longest was toluene, tri-n-decylamine, tridodecylamine, squalane, and tetrahydrofuran. However, SAXS analysis showed that Comb PMA expanded in both toluene and tetrahydrofuran, and the general relationship of molecular expansion in solvents with high solubility and contraction in solvents with low solubility was not established. The HSP values of Comb PMA in 34 different solvents were determined using a solubility test, but it was not possible to determine whether the solubility of the main chain or the side chains of Comb PMA determines the solubility of Comb PMA itself. The Combs PMA used in this study has longer side chains than general-purpose PMA, but the main chain is 25 times longer than the side chains, so the structural analysis by SAXS is considered to reflect mainly the structure of the main chain.

Therefore, we divided Comb PMA into main chains and side chains and determined their HSP values. Polymethyl methacrylate was used as a model for the main chain and polyethylene as a model for the side chains, and the HSP values from the database were used. As a result, the structure of Comb PMA was found to be as follows, depending on the solubility in the base oil to which it is added. (1) In a base oil with low solubility of the main chain and high solubility of the side chains, the main chain of the Comb PMA molecule shrinks and the side chains expand. (2) In a base oil with high solubility of both the main chain and side chains, both the main chain and side chains expand. (3) In a base oil with low solubility of the main chain but even lower solubility of the side chains, the contraction of the side chains prevents the contraction of the main chain.

In addition, when the viscosity index of the solutions with each pure solvent and Comb PMA was examined, a remarkable viscosity index improvement effect was observed in the solvent in which the main chain of Comb PMA was shrunk at 25°C. The viscosity index of the solution with Comb PMA was higher in the solvent in which the main chain of Comb PMA was shrunk at 25°C than in the pure solvent in which the main chain was shrunk.

CO12-12 Nanostructural Analysis of Lubricant/Metal Interface by Neutron Reflectometry

T. Hirayama, N. Yamashita[1] and M. Hino[2]

Graduate School of Engineering, Kyoto University
[1]Graduate School of Engineering, Kyoto University
[2]Institute for Integrated Radiation and Nuclear Science, Kyoto University

INTRODUCTION: Our research group has focused on ester derivatives, which are ashless lubricant additives, and has evaluated their tribological properties. In high-speed reciprocating friction and wear tests, this additive has been found to have the same friction-reducing effect as glycerin monooleate at room temperature and the same wear-inhibiting effect as ZDDP and phosphate ester amine salts at high temperatures.

In this study, we focused on additives with enhanced adsorption performance by introducing an oxyalkylene (AO) group between the ester carbonyl and alkyl groups of the ester derivative. In general, it is known that the adsorption performance of additives decreases when the moisture content in lubricating oil is low. Therefore, in this study, the difference in adsorption performance between lubricants with and without AO groups was verified by using lubricants with low moisture content. Specifically, the structure of the adsorption layer and friction characteristics were evaluated by neutron reflectometry and AFM friction measurements.

SAMPLES: In this study, an oxyalkylene group (FM-1) was added to a certain ester derivative (FM-0) used in the previous study. For the neutron reflectometry, these additives were added to deuterated hexadecane at a concentration of 0.1 wt%, and for the AFM friction measurement, each additive was added to polyalpha olefin (50 cSt@40°C) at a concentration of 0.1 wt%.

NEUTRON REFLECTOMETRY: A substrate with a thickness of about 30 nm of iron deposited on the surface of a 50 × 50 × 10 mm silicon block using a sputtering system was used. BL16 SOFIA at MLF in J-PARC was used for the NR measurement. Table 1 shows the analysis results of the data measured at 25°C after 30 minutes in a drop of lubricating oil. In the neutron reflectometry, fitting analysis was performed assuming a simplified layer structure model. Therefore, although it is necessary to allow for some errors in the results when the actual film structure is complex, there were no significant differences in the adsorption layer structures formed by FM-0 and FM-1. Considering that oleic acid, which has the same alkyl chain length as the additive used in this study, generally forms an adsorption layer of about 2 nm, the thickness of the film formed by FM-0 and FM-1 is more than 3 nm, although the polar groups are different, suggesting that the adsorption layers may not be simple single-layer structures.

Table 1. Film structure formed by additives.

	Thickness, nm	Film density, %
FM-0	3.0	47
FM-1	3.1	44

FRICTION TEST: To evaluate the friction and wear properties of each additive, friction tests were conducted using an AFM (SPM-9700, Shimadzu). Cantilevers (AIOAL-TL-B, BudgetSensors) with 8 μm diameter silica spheres bonded to them were used for the measurements. The experimental procedure is described below.

(i) A drop of each lubricant was placed on a silicon chip on which iron had been deposited by a sputtering machine, and the chip was placed in the AFM.
(ii) The area was scanned at a surface pressure of approximately 400 MPa and a speed of 40 μm/s, and 100 images (128 lines/image) of a 2 × 2 μm area were acquired.

An example of the results obtained is shown in Fig. 2. In particular, the friction coefficient of FM-1 shows a small value immediately after the start of friction, indicating that the fluctuation is small. This indicates that the AO groups introduced into the material increase the adsorption strength on the iron surface, which may increase the stability against friction. Thus, the combination of the neutron reflectometry and the friction test is an example of how the neutron reflectometry can contribute to the advancement of tribological research.

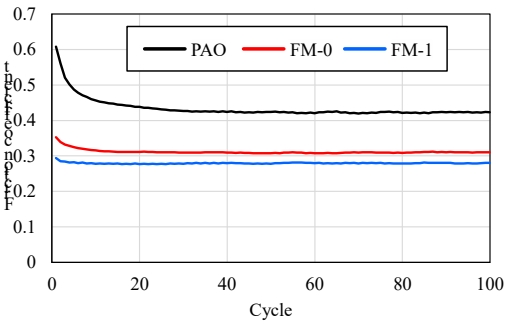

Fig. 2. Friction coefficients of interface with additives.

CO12-13 Study of Isotope Separation via Chemical Exchange Reaction

R. Hazama, P. Kumsut, T. Yoshimoto, A. Rittirong[1], C. Pitakchaianan, K. Kosinarkaranun, Y. Sakuma[2], T. Fujii[3], T. Fukutani[4], Y. Shibahara[4], T. Kishimoto[1]

Graduate School of Human Environment, Osaka Sangyo University,
[1]Research Center for Nuclear Physics, Osaka University,
[2]Laboratory for Advanced Nuclear Energy, Tokyo Institute of Technology,
[3]Graduate School of Engineering, Osaka University
[4]Institute for Integrated Radiation and Nuclear Science, Kyoto University

INTRODUCTION: Chemical isotope separation for calcium and lithium has been studied by liquid-liquid extraction (LLE) with DC18C6 crown-ether [1,2]. This report describes distribution coefficient (D) for chemical equilibrium (reaction time) of the two phase (aqueous and organic) reaction of LLE.

EXPERIMENTS: Chemical Isotopic exchange occurs according to the following chemical exchange reaction:
$^{40}Ca^{2+}_{(aq)} + {}^{48}CaL^{2+}_{(org)} \rightarrow {}^{48}Ca^{2+}_{(aq)} + {}^{40}CaL^{2+}_{(org)}$ (1)
, where L represents macrocyclic polyether(18-crown-6). Calcium chloride solution (30% w/w $CaCl_2$ (aq), and $CaCl_2$) was mixed in an Erlenmeyer flask with 0.07M DC18C6 in chloroform, by the volume ratio of 20/200 mL (aq/org), for 1 second, 1, 10, 30, and 60 minute. The mixture solution was put in the separating funnel for 10 minutes before separation. The water volume for back extraction is 1/10 of the volume ratio of water to organic phase after extraction.

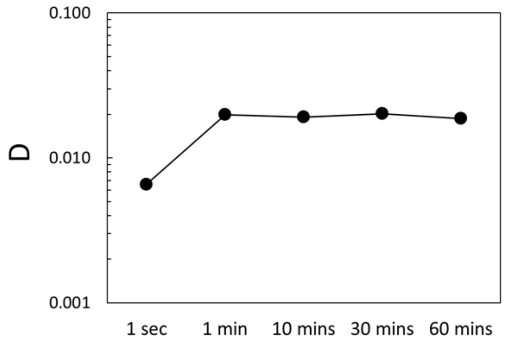

Fig. 1. Distribution coefficient (D) of Ca isotope on various extraction time using DC18C6 crown-ether: Preliminary.

In the case of lithium, K. Nishizawa et al. [3] reported the equilibria chemical exchange of lithium (LiCl) and in the organic solution contained B15C5 crown-ether to be 0.0029. The distribution coefficient was one order smaller than our finding (0.0292±0.0001). The reason was that the extraction system was different. K. Nishizawa used 20 mL of 0.186 M B15C5 and 20 mL of 8.0M LiCl (volume ratio (aq/org) = 1/1), while our experiment was 200 mL 0.07M DC18C6 and 20 mL 8.4M LiCl (volume ratio (aq/org) = 1/10).

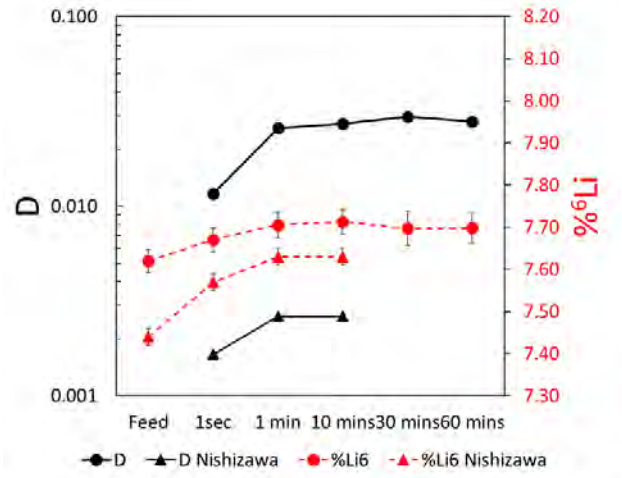

Fig. 2. Comparison between our result and K. Nishizawa et al. [3] on the isotope separation of lithium using B15C5 crown-ether: Preliminary.

RESULTS: The distribution coefficient (D) results indicate that the chemical exchange between ion and crown-ether becomes equilibrium on a magnetic stirrer's extraction time of at least 1 minute. This finding is in good agreement with K. Nishizawa et al. [3] on the study of the isotope separation via liquid-liquid extraction of lithium isotope. Their finding indicated that the chemical equilibria of 5 seconds and isotope equilibria at 30 seconds by mixing stirrer. Compared to our experiments, the extraction time was studied from 1 second and 1 minute, implying that the extraction at 1 minute using a magnetic stirrer is sufficient for equilibria the chemical and isotope exchange. The finding could benefit the shortened time required for micro-reactor extraction [4]. Fig 2 shows the comparison between this research and K. Nishizawa et al. in terms of D and %^{6}Li in the organic phase.

REFERENCES:

[1] A. Rittirong, Doctor Thesis, OSU (2022).
[2] A. Rittirong *et al.,* J. Phys.: Conf. Ser., **2147** (2022) 012015.
[3] K. Nishizawa *et al.,* J. Nucl. Sci. Technol., **218(9)** (1984) 694.
[4] R. Hazama *et al.,* KURRI Progress Report 2018 (2019) 252, KURRI Progress Report 2019, (2020) 282.

CO12-14 Development of neutron phase imaging system with Talbot-Lau interferometer for medium power reactor source

Y. Seki, T. Samoto, R. Nakamura[1], M. Hino[1]

Institute of Multidisciplinary Research for Advanced Materials, Tohoku university
[1]Institute for Integrated Radiation and Nuclear Science, Kyoto University

INTRODUCTION: The neutron phase imaging technique [1] offers high-sensitivity and microscopic information on samples that cannot be obtained using conventional absorption imaging techniques. Among various methods, the Talbot-Lau (TL) interferometry, a type of grating interferometry, is widely used worldwide. This method has advantages for use in medium reactor sources such as KUR. Compared to crystal-based methods, TL interferometry requires relatively mild spatial and temporal coherence conditions, which enables the use of white beams without the need to collimate incident beams narrowly. We have recently installed a neutron phase imaging system based on the TL interferometer at the CN-3 port.

EXPERIMENTS: In this experiment, we have specifically developed a new absorption grating (G2) with a large area of 64 × 64 mm^2 for the TL interferometer. The absorption lines were formed on a silicon mold using the oblique evaporation technique of gadolinium [1, 2]. By precisely adjusting the evaporation angle and repeating gradual deposition, we achieved a thick gadolinium line with a thickness of 20 μm. The performance of this new G2 was evaluated experimentally at the CN-3. Additionally, utilizing the TL interferometry, we observed a carbon steel (JIS S45C) disk subjected to high-pressure torsion (HPT) process, which introduces shear strains and refines the grain size of the material.

RESULTS: An observed neutron transmission of G2 is presented in Fig. 1. The average transmission in the grating region was 0.5, consistent with the design value. A visibility map of the interference pattern is depicted in Fig. 2 with an average value of 49%. This result is also in good agreement with the theoretical value obtained by assuming the wavelength spectrum at the CN-3.

Figure 3 displays resultant visibility images of the samples. For comparison, a disk without undergoing the HPT process was simultaneously observed. The visibility images indicate the degree of small angle scattering by microstructures in the sample, whose size is characterized by an auto-correlation length. At an auto-correlation length of 1.2 μm (Fig. 3(a)), the visibility of the unprocessed disk is higher than that of the processed one. Conversely, at an auto-correlation length of 3.8 μm (Fig. 3(b)), the visibility of the non-processed disk is lower than the other, whose visibility remains unchanged. These results suggest that the HPT process effectively reduces the grain size in the disk to less than about 1 μm.

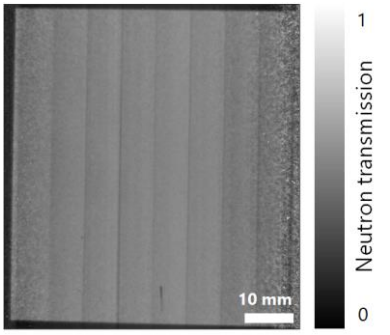

Fig. 1. Neutron transmission of the new G2.

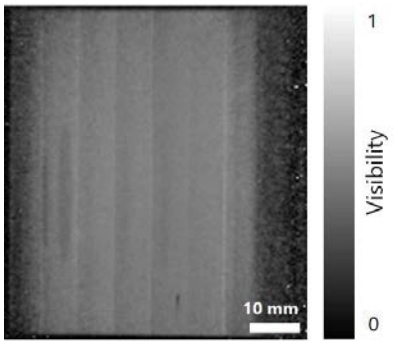

Fig. 2. Visibility map of interference pattern of the TL interferometer including the new G2.

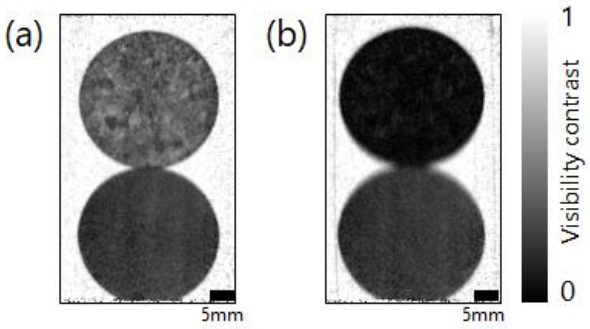

Fig. 3. Visibility images of carbon steel disks. The upper and lower disks are unprocessed and pressed by HPT, respectively. (a) auto-correlation length is 1.2 μm. (b) auto-correlation length is 3.8 μm.

REFERENCES:

[1] T. Samoto *et al.*, Jpn. J. Appl. Phys., **58** (2019) SDDF12.
[2] T. Samoto *et al.*, Mater. Sci. Semicond., **92** (2019) 91-95.

CO12-15 Fiber-reading Radiation Monitoring System with an Optical Fiber and Red-emitting Scintillator at the ^{60}Co Radiation Facility III

S. Kurosawa[1,2,3], C. Fujiwara[2,4], D. Matsukura[2,4], S. Ishizawa[2], A. Yamaji[1,2], T. Takata[5], H. Tanaka[5]

[1]*New Industry Creation Hatchery Center, Tohoku University*
[2] *Institute for Materials Research Tohoku University*
[3] *Institute of Laser Engineering, Osaka University*
[4] *Department of Materials Science, Graduate School of Engineering, Tohoku University*
[5] *Institute for Integrated Radiation and Nuclear Science, Kyoto University*

INTRODUCTION: Decommissioning reactors at nuclear power plant safety is an important issue, and a real-time dose-rate monitor in extremely high radiation dose conditions is required. We have proposed a dose-rate monitor system consisting of a scintillator, optical fiber and Charge Coupled Device (CCD) spectrometer, and scintillation photons through the fiber are read under the lower dose condition with the CCD. As we mentioned in the previous reports [1-2], the scintillator is required to have a long-emission wavelength (550 – 1,000 nm) and (ii) high light output (over 40,000 photons/ thermal neutron).

Cs_2HfI_6 (CHI) has a high light output (over 60,000 photons/MeV), high effective-atomic number (over 60), red and infrared emission (600 – 800 nm) and no afterglow (less than 1% within 1s), and this material is available for such dose monitors [1][3].

However, CHI has insufficient sensitivity to neutrons. Neutrons from ^{244}Cm and ^{242}Cm are assumed to exist inside the reactors, and we focused on Li_2HfBr_6 and other candidates [4].

EXPERIMENTS: Row materials powders were inserted in a quartz ampoule in Ar gas atmosphere. The ampoule was evacuated and sealed off by an oxyhydrogen burner, and the crystals were grown by the vertical Bridgman-Stockbarger method.

Using the scintillator, we operated the demonstration of the dose-rate monitoring system under high neutron and gamma-ray intensity at The Heavy Water Neutron Irradiation Facility (HWNIF) or research reactors (KUR) and the ^{60}Co facility, respectively. The scintillation spectra were measured for the sample with a neutron flux of around 6.0×10^{8}-4.0×10^{6} n cm^{-2}s^{-1} using a CCD through the optical fiber with a length and core diameter of 20 m and 0.6 mm, respectively.

RESULTS: We succeeded in growing the Li_2HfBr_6 crystal, and the single phase was confirmed by the result of the powder X-ray diffraction. Li_2HfBr_6 had an emission wavelength of around 600 nm excited by X-rays and light output of around 50,000 photons/ thermal neutron.

Li_2HfBr_6 had emission peaks at approximately 600 nm excited by gamma rays from the ^{60}Co source, the dose-rate dynamic range for the monitor system was up to a few kGy/h.

Scintillation spectra for the Li_2HfBr_6 sample irradiated with neutrons under the 6.0×10^{8}~4.0×10^{6} neutrons cm^{-2}s^{-1}. Figure 1 shows the emission spectrum for Li_2HfBr_6 under the 6.0×10^{8} neutrons cm-2s-1, and the emission band was observed at around 600 nm. In addition, we measured the emission spectrum without the scintillator as background evaluations, and no signal was observed as shown in Fig. 1.

To detect gamma rays, we also measured other scintillation materials, instead of Li_2HfBr_6, with a lower detection efficiency for neutrons. The result shows no significant signal excited by gamma rays was observed. The signal intensities, defined as the integration of the emission spectrum, as a function of neutron flux were fitted by the power law function.

Thus, the dose-rate monitor system with Li_2HfBr_6 can be applied to both gamma-ray and neutron monitors.

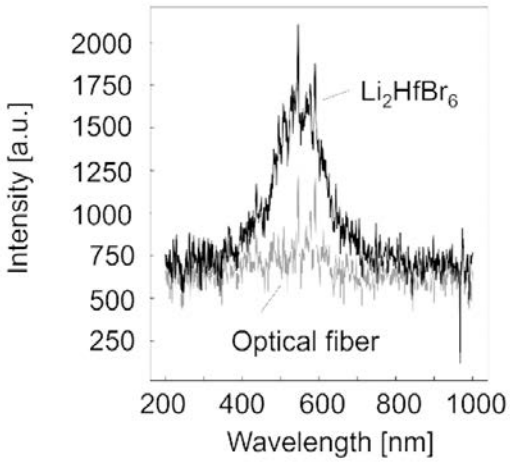

Fig. 1. Emission spectra of the dose-rate monitor system with Li_2HfBr_6 and without the crystal; the signal was generated from only optical fiber.

REFERENCES:

[1] S. Kurosawa *et al.*, KURNS PROGRESS REPORT 2020 (2021) 79.
[2] S. Kurosawa *et al.*, KURNS PROGRESS REPORT 2021 (2022) 248.
[3] S. Kodama *et al.*, Ra-diat. Meas., **124** (2019) 54-58.
[4] JAEA&IRID report (in Japanese). https://www.meti.go.jp/earthquake/nuclear/decommissioning/committee/osensuitaisakuteam/2016/11/3-04-03.pdf.